Frequency-dependent shear viscosity, sound velocity, and sound attenuation near the critical point in liquids. II. Comparison with experiment

R. Folk[1] and G. Moser[2]
[1]*Institute for Theoretical Physics, University of Linz, Linz, Austria*
[2]*Institute for Physics and Biophysics, University of Salzburg, Salzburg, Austria*
(Received 23 December 1996)

We compare the theoretical results of an explicit one loop calculation of the critical behavior of the sound propagation in pure liquids near the gas-liquid critical point, which has been derived within the field-theoretic renormalization group formalism, with experimental data in ^{3}He, ^{4}He, CO_2, SF_6, and Xe. The nonuniversal initial values of two dynamic model parameters, which are necessary for the calculation of all theoretical expressions, are determined by a fit of the shear viscosity at zero frequency in a small temperature region. The static quantities appearing in the theoretical expressions are taken from experiment. With these two dynamical initial values the temperature flow of the dynamic model parameters is completely determined. The sound attenuation and the sound velocity at arbitrary frequency as well as the thermal conductivity or the thermal diffusion coefficient may be calculated without any adjustable parameter. The parameter free predictions are in very good agreement with experimental results. This also holds for scaling plots of the reduced attenuation and dispersion taking into account the nonasymptotic behavior of the dynamic scale. [S1063-651X(97)04712-0]

PACS number(s): 62.60.+v, 64.70.Fx, 64.60.Ht, 05.70.Jk

I. INTRODUCTION

In the first part of the present work [1] (referred to as paper I in the following) we have derived theoretical expressions for several transport coefficients within an extension of the dynamic model H including fast sound modes. Model H has been introduced by Siggia, Halperin, and Hohenberg [2] to describe the effects of the order parameter fluctuations on the dynamics of the slow heat and shear modes in liquids near the critical point. The extension allows the calculation of these effects on sound propagation. For the calculation of the critical behavior of the thermal conductivity and the shear viscosity it is sufficient to consider the dynamical equations for the entropy density and the transverse momentum density. For the calculation of the sound mode one has to add the equations for the mass density and the longitudinal momentum density to model H [3,4]. Within the field theoretic renormalization group theory we have derived expressions for the shear viscosity, the thermal conductivity, the sound velocity, and the sound attenuation valid in a temperature region from the transition temperature T_c to the background region (where the transport coefficients behave analytically). We also calculated the sound mode transport coefficients at finite frequencies.

The aim of this work is to compare the theoretical expressions for the hydrodynamic transport coefficients with their experimental counterparts and to locate nonasymptotic effects. Here we concentrate on the critical sound propagation; the shear viscosity will be considered in a future work. In the comparison with experiment some quantities have to be taken as input in the theoretical expressions; other parts depend on the renormalization group calculation. So we have two sources of uncertainties in our predictions on the experimental side as well as on the theoretical side (e.g., loop expansion). The experimental information about static thermodynamic derivatives and one hydrodynamic coefficient at zero frequency is sufficient for the determination of all dynamical background parameters entering the theoretical expressions. The remaining hydrodynamic coefficients at zero frequency as well as at finite frequencies may then be calculated without any additional parameters. This program is quite generally applicable and has been first developed for the critical dynamics near the superfluid transition (see the review [5] and [6]).

Our detailed analysis of the theory is restricted to those liquids for which measurements of several transport coefficients are available (i) for the determination of the background parameters and (ii) to test the predictions of the theory. Especially for item (i) one needs data in an adequate accuracy and over a sufficiently large region of temperature further away from T_c. So far only asymptotic scaling functions have been considered in the comparison with experiment. After first attempts [7,8], Ferrell and Bhattacharjee [9,10] have found within a mode coupling theory agreement of experiment with their asymptotic results. However, only the ultrasonic attenuation in one wavelength at the critical point of pure fluids was explicitly presented [10]. Very recently a comparison with an asymptotic two loop calculation (with adjustable frequency scale and scale of the reduced attenuation and dispersion) has been performed [11]. We take into account nonasymptotic effects in the transport coefficients and the measurements indeed show these effects in the experimental region. For the sound modes one may introduce scaling variables, not necessarily in the form of asymptotic expressions like the characteristic temperature-dependent frequency [12], and calculate scaling functions even in the nonasymptotic region.

Recently much progress has also been made within mode coupling theory concerning the transport coefficient shear viscosity and thermal conductivity [13]. Mode coupling theory calculates the critical part of the transport coefficients using an ansatz according to the dynamic scaling theory, whereas in our approach, presented in paper I, the background values of the transport coefficients are included. We note that the mode coupling result mentioned includes also the wave vector dependence of the nonhydrodynamic region.

The paper is organized as follows: In Sec. II we write down the one loop expressions of the thermal conductivity, the shear viscosity at zero frequency in a form suitable for use in the comparison with experiment. We also need the solution of the corresponding flow equations for the two independent dynamic model parameters appearing in these transport coefficients. In Sec. III we summarize the results of the model on the sound velocity and the sound attenuation derived in paper I. The one loop expressions as a function of the reduced temperature and the frequency, where static model parameters are replaced by experimentally measurable thermodynamic derivatives, are given explicitly. Further we discuss the matching conditions that connect the flow parameter with the reduced temperature. In Sec. IV we determine the static parameters appearing in the model Hamiltonian from experimentally measurable quantities. The method is quite analogous to the one used at the λ transition in ^{4}He [14] and ^{3}He-^{4}He mixtures [15]. In Sec. V we determine the dynamical background parameters by fitting experimental shear viscosity data over a restricted temperature interval in the background (apart from one example where we use the thermal diffusion coefficient). For some liquids we then show the predictions for the thermal diffusivity or thermal conductivity. Finally we compare our predictions with the measurements of the sound velocity and the sound attenuation. In Sec. VI we calculate the nonasymptotic scaling functions and compare them with the reduced dispersion and attenuation. Some concluding remarks close this paper.

II. SHEAR VISCOSITY AND THERMAL CONDUCTIVITY AT VANISHING FREQUENCY

In Eq. (6.6) of the preceding paper [1], abbreviated as Eq. (I.6.6), we have derived the theoretical expressions of the shear viscosity $\overline{\eta}$,

$$\overline{\eta}(t)=\frac{1}{RT}\xi^{-2}(t)\lambda_t(t)[1+E_t(\{\Xi(t)\})] \tag{2.1}$$

with T the temperature and R the gas constant (we always take $T=T_c$ in the calculations). From the thermal conductivity κ_T at vanishing frequency one obtains the thermal diffusion coefficient

$$D_T(t)=\frac{\kappa_T(t)}{\rho C_P(t)} \tag{2.2}$$

with the density ρ and the isobaric specific heat $C_P(t)$. Inserting (I.6.5) for the conductivity we get

$$D_T(t)=\xi^{-2}(t)\Gamma(t)\hat{\Gamma}_{\phi\phi}(u(t))[1+G(\{\Xi(t)\})]. \tag{2.3}$$

Both transport coefficients are proportional to the inverse squared correlation length ξ and the corresponding Onsager coefficients λ_t and Γ. The perturbational contributions are contained in the functions E_t and G, which depend on the set of couplings $\{\Xi(t)\}=\{\gamma_q(t),u(t),f_t(t)\}$. γ_q is the coupling between the order parameter and the density fluctuations introduced in (I.2.10) and u is the fourth order coupling of the corresponding ϕ^4 model (I.2.18). f_t is the mode coupling parameter (I.5.4) between the order parameter fluctuations and the transverse momentum density. In the thermal diffusion also the static vertex function $\hat{\Gamma}_{\phi\phi}$ appears. All quantities mentioned depend on the relative temperature distance $t=(T-T_c)/T_c$ to the transition temperature T_c. In one loop order the expressions for the transport coefficients reduce with (I.6.7) to

$$\overline{\eta}(t)=\frac{1}{RT}\xi^{-2}(t)\lambda_t(t)\left[1-\frac{f_t^2(t)}{36}\right], \tag{2.4}$$

$$D_T(t)=\xi^{-2}(t)\Gamma(t)\left[1-\frac{f_t^2(t)}{16}\right]. \tag{2.5}$$

In Eqs. (2.4) and (2.5) three temperature-dependent dynamic parameters $\Gamma(t)$, $\lambda_t(t)$, and $f_t(t)$ appear but only two of them are independent. Choosing $\Gamma(t)$ and $f_t(t)$ as independent $\lambda_t(t)$ is determined by inverting (I.5.4):

$$\lambda_t(t)=\frac{g^2(t)}{f_t^2(t)\Gamma(t)}. \tag{2.6}$$

From (I.4.23) one can see that the mode coupling g renormalizes only in a trivial manner, therefore the solution of its flow equation is of the simple form (in $d=3$)

$$g(l)=A_d^{1/2}(\kappa l)^{-3/2}\mathring{g}. \tag{2.7}$$

As discussed in paper I we choose the wave number κ and the connection between the flow parameter l and the reduced temperature as

$$\kappa=\xi_0^{-1}, \quad l=\xi_0\xi^{-1}(t). \tag{2.8}$$

The geometrical factor A_d at three dimensions is $A_3=1/4\pi$. Inserting Eq. (2.8) and the unrenormalized mode coupling (I.2.7) into Eq. (2.7) the temperature dependence of g in $d=3$ reads

$$g(t)=\frac{RT}{\sqrt{4\pi N_A}}\xi^{3/2}(t). \tag{2.9}$$

Inserting Eqs. (2.6) and (2.9) into the shear viscosity (2.4) we get the final expression used in the following:

$$\overline{\eta}(t)=\frac{RT}{4\pi N_A}\frac{\xi(t)}{f_t^2(t)\Gamma(t)}\left[1-\frac{f_t^2(t)}{36}\right]. \tag{2.10}$$

The flow of the remaining two parameters Γ and f_t is determined by (I.4.36) and (I.4.40). With Eq. (2.8) the flow parameter may be replaced by the reduced temperature. Inserting the one loop ζ functions (I.6.14) the resulting flow equations are

$$\frac{d\Gamma}{dt}=\frac{3}{4}\xi^{-1}(t)\xi'(t)\Gamma(t)f_t^2(t) \tag{2.11}$$

$$\frac{df_t}{dt}=\frac{1}{2}\xi^{-1}(t)\xi'(t)f_t(t)\left(1-\frac{19}{24}f_t^2(t)\right), \tag{2.12}$$

where we have introduced the derivative $\xi'(t)=d\xi/dt$. In this form one recognizes that the solutions of Eqs. (2.11) and (2.12) reach constant values in the background because of $\xi'(t)=0$. The equations are easily integrated and have the solutions

$$\Gamma(t)=\Gamma_0\left\{\frac{19f_0^2\xi(t)}{24\xi(t_0)}\left[1+\frac{\xi(t_0)}{\xi(t)}\left(\frac{24}{19f_0^2}-1\right)\right]\right\}^{18/19}, \quad (2.13)$$

$$f_t^2(t)=\frac{24}{19}\left[1+\frac{\xi(t_0)}{\xi(t)}\left(\frac{24}{19f_0^2}-1\right)\right]^{-1}, \quad (2.14)$$

with the initial conditions $\Gamma(t_0)=\Gamma_0$ and $f_t(t_0)=f_0$ at $t=t_0$. Expanding Eq. (2.14) in the asymptotic region leads to the approximation by the first transient (exponent $\omega_f=1$ in one loop order)

$$f_t^2(t)=\frac{24}{19}\left[1-\frac{\xi(t_0)}{\xi(t)}\left(\frac{24}{19f_0^2}-1\right)\right]. \quad (2.15)$$

The nonuniversal amplitude of the transient is fixed by the initial values t_0 and f_0^2. However, this approximation is restricted to a certain region near the fixed point (see for an example Fig. 5).

Inserting the solutions (2.13) and (2.14) the temperature flow of the thermal diffusivity (2.5) and the shear viscosity (2.10) is completely determined. All we need at this stage are the two initial values Γ_0 and f_0 and an explicit expression for the correlation length $\xi(t)$. The temperature dependence of the correlation length in general does not follow the asymptotic power law but may include corrections to the leading terms in the crossover region to its constant background value ξ_b. It would be worthwhile to measure the explicit crossover temperature dependence of $\xi(t)$ in order to perform the analysis in the background properly. However, lacking more detailed experimental information we will use the asymptotic expression

$$\xi(t)=\xi_0 t^{-\nu}, \quad (2.16)$$

which seems to be sufficient in the temperature region $t\leqslant 10^{-1}$ and with respect to the uncertainties of other physical quantities entering the transport coefficients. The value of the universal critical exponent $\nu=0.63$ [2] has been experimentally confirmed for several liquids [16]. Thus we need for the calculation of the shear viscosity and the thermal diffusivity the knowledge of three nonuniversal parameters, ξ_0, Γ_0, and f_0. The amplitude of the correlation length ξ_0 has been determined experimentally for several fluids, and is listed together with the critical temperature T_c and the critical density ρ_c for the liquids considered in the following in Table I. For a comprehensive overview on experimental results in several other liquids see [16] and the references therein.

In the asymptotic region the order parameter Onsager coefficient obeys a power law $\Gamma(t)=\Gamma_{as}t^{-(18/19)\nu}$ with the amplitude

$$\Gamma_{as}=\Gamma_0\left(\frac{19}{24}f_0^2t_0^{\nu}\right)^{18/19}, \quad (2.17)$$

TABLE I. Critical parameters of several fluids.

Liquid	ξ_0 (Å)	T_c (K)	ρ_c (g/cm^3)
C_2H_6	1.8	305.33	0.2065
^{3}He	2.7	3.310	0.0415
^{4}He	2.0	5.190	0.0696
Xe	1.9	289.73	1.110
CO_2	1.6	304.13	0.4678
SF_6	2.0	318.69	0.730

whereas $f_t^2(t)$ reaches its fixed point value $f_t^{2\star}=\frac{24}{19}$. Thus the different asymptotic amplitudes of the shear viscosity and the thermal diffusion coefficient are determined by ξ_0, and Γ_{as} according to Eqs. (2.3) and (2.10), but not by Γ_0 and f_0 separately.

The initial values of the Onsager coefficient Γ_0 and the mode coupling f_0 may be found by fitting the experimental data of one of the two hydrodynamic coefficients $\overline{\eta}$ or D_T by the corresponding theoretical expression over a sufficient nonasymptotic temperature interval (in order to get f_0). The second hydrodynamic coefficient then can be predicted without any further experimental input.

For the calculation of the thermal conductivity from the dynamic model one needs according to Eqs. (2.2) and (2.5) the isobaric specific heat $C_P(t)$ and the mass density ρ. The mass density ρ is a smooth function of the temperature and therefore may be replaced in the considered narrow temperature region near T_c by the critical density ρ_c. Because C_P is not directly measurable in experiments it is necessary to relate it to measurable thermodynamic derivatives. Details concerning the explicit calculation of C_P from experimental data are discussed in Sec. IV.

III. SOUND ATTENUATION AND SOUND VELOCITY

Let us now turn to the sound attenuation and the sound velocity and summarize the results of paper I. The sound attenuation $\alpha(t,\omega)$ is related to the sound diffusion coefficient D_s and the sound velocity c_s by

$$\alpha(t,\omega)=\frac{\omega^2}{2c_s^3(t,\omega)}D_s(t,\omega). \quad (3.1)$$

A closer examination of the magnitudes of the different fluctuation contributions to the sound velocity and the sound diffusion shows that the contributions of the thermal conductivity and the bulk viscosity (I.5.23) are negligible compared to the contribution related to the frequency-dependent $\langle\phi^2\phi^2\rangle$ correlation function (I.5.20) in the asymptotic region [3]. In the background, however, only these neglected terms lead to a finite background value of $D_s(t,\omega=0)$ [see (I.6.26)] and to the finite (hydrodynamic) background value of the attenuation. Usually this background value is already subtracted in the experimental presentations and therefore we only consider the leading fluctuating part of the sound attenuation, which reaches zero for all frequencies in the background. The sound velocity reduces to the adiabatic compressibility in the background [see (I.6.19)]. Thus we may simply write

$$c_s^2(t,\omega)=\mathrm{Re}[\mathcal{C}_s^2(t,\omega)],\quad D_s(t,\omega)=-\frac{1}{\omega}\mathrm{Im}[\mathcal{C}_s^2(t,\omega)],\quad (3.2)$$

with the complex coefficient $\mathcal{C}_s^2$ given by [see (I.5.20)]

$$\mathcal{C}_s^2(t,\omega)=\frac{a_j a_q(\xi_0^{-1}l)^6 c^2(l)}{1+[\gamma_q^2(l)/a_q]F_+(v(l),w(l),\{\Xi(l)\})}.\quad (3.3)$$

The ϵ-expanded one loop expression of $F_+(v(l),w(l),\{\Xi(l)\})$ is [see (I.5.6) and (I.5.18)]

$$F_+(v(l),w(l),\{\Xi(l)\})$$
$$=-\frac{1}{4}\left\{\frac{v^2}{v_+v_-}\ln v+\frac{1}{v_+-v_-}\left[\frac{v_-^2}{v_+}\ln v_- -\frac{v_+^2}{v_-}\ln v_+\right]\right\}.\quad (3.4)$$

with

$$v_\pm(l)=\frac{v(l)}{2}\pm\sqrt{\left(\frac{v(l)}{2}\right)^2+iw(l)}.\quad (3.5)$$

From (I.5.3) the temperature parameter $v(l)$ and the frequency parameter $w(l)$ are

$$v(l)=\frac{\xi^{-2}(t)}{(\xi_0^{-1}l)^2},\quad w(l)=\frac{\omega}{2\Gamma(l)(\xi_0^{-1}l)^4}\quad (3.6)$$

The calculation of the static coupling $\gamma_q^2(l)/a_q$ will be described in Sec. IV. Finally from (I.2.7), (I.4.36), and (I.2.25) we have for the parameter $c^2(l)$ the expression

$$c^2(l)=(RT\rho)^2(\xi_0^{-1}l)^{-6}Z_q^{-1}e^{\int_1^l(dx/x)\zeta_q}.\quad (3.7)$$

The parameter c renormalizes with a static renormalization factor Z_q, which may be eliminated using the static correlation it function (I.4.18). From this relation it follows that

$$Z_q^{-1}e^{\int_1^l(dx/x)\zeta_q}=\frac{\mathring{\Gamma}_{qq}^{(s)}(\xi^{-2},\mathring{\gamma}_q,\mathring{u})}{\hat{\Gamma}_{qq}^{(s)}(\gamma_q(l),u(l))}.\quad (3.8)$$

Inserting (I.2.17) for the unrenormalized vertex function and (I.4.19) for the amplitude functions we get

$$Z_q^{-1}e^{\int_1^l(dx/x)\zeta_q}=\frac{1+[\gamma_q^2(l)/a_q]F_+^{(s)}(u(l))}{a_q\langle q_0q_0\rangle_c}.\quad (3.9)$$

The unrenormalized correlation function in Eq. (3.9) may be replaced by the corresponding thermodynamic derivative using Eq. (I.2.14). With Eq. (3.9) the parameter (3.7) turns into

$$c^2(l)=\frac{RT\rho}{a_q}(\xi_0^{-1}l)^{-6}\left(\frac{\partial P}{\partial\rho}\right)_\sigma\left(1+\frac{\gamma_q^2(l)}{a_q}F_+^{(s)}(u(l))\right).\quad (3.10)$$

The flow parameter l, now considered at finite frequencies, is a function of the temperature distance t and the frequency ω. It is determined by the matching condition (I.2.28)

$$\xi^{-8}(t)+\left(\frac{2\omega}{\Gamma(l)}\right)^2=(\xi_0^{-1}l)^8.\quad (3.11)$$

Equation (3.11) includes the Onsager coefficient $\Gamma(l)$. With the initial condition Γ_0 from the viscosity fit in the preceding section and the flow equation (2.11) we know the Onsager coefficient as a function of the temperature distance $\bar{t}$ at $\omega=0$, where we have introduced the bar to avoid confusion with the temperature distance t at finite frequency. A given temperature distance t at finite frequency corresponds to a certain value $l(t,\omega)$. The same value of the flow parameter on the other side may be written as an effective temperature distance $\bar{t}$ at $\omega=0$ by the relation (2.8) $l=\xi_0\xi^{-1}(\bar{t})$ [this only works when $\xi(\bar{t})$ is a bijective function, which is the case for the analysis performed here [17]]. Therefore it is sufficient to know the Onsager coefficient $\Gamma(\bar{t})$ for the $\omega=0$ temperature scale (the same holds for all other static and dynamic parameters of the model). Via Eqs. (2.8) and (3.11) all model parameters are known as a function of t at arbitrary frequencies. Inserting Eq. (2.8) into Eq. (3.11) the two temperature scales are directly related by

$$\xi^{-8}(t)+\left(\frac{2\omega}{\Gamma(\bar{t})}\right)^2=\xi^{-8}(\bar{t}).\quad (3.12)$$

The above equation allows one to calculate for each temperature distance t at finite frequency the corresponding effective temperature distance $\bar{t}$ at $\omega=0$ at which the values of the model parameters have to be known. Because the correlation length is a static quantity, it has to be the same function of the temperature distance independent of the frequency, which means that we may write analogous to Eq. (2.16) $\xi(\bar{t})=\xi_0\bar{t}^{-\nu}$ in the asymptotic region. Inserting in Eq. (3.12) we get

$$t^{8\nu}+\left(\frac{2\xi_0^4\omega}{\Gamma(\bar{t})}\right)^2=\bar{t}^{8\nu}.\quad (3.13)$$

In Fig. 1 the function $\bar{t}(t)$, calculated by inversion of Eq. (3.13) at fixed ω, is shown at several frequencies. Approaching the critical temperature at finite frequencies ($t\to0$), the corresponding effective temperature distance at zero frequency $\bar{t}$ becomes a constant. Thus all static and dynamic parameters that are functions of the flow parameter also turn into constant values at T_c. The temperature distance t at which these parameters cross over to constant values depends on the frequency.

With the solution $\bar{t}(t,\omega)$ of (3.13) the temperature and frequency parameter (3.6) can be rewritten as

$$v[t,\bar{t}]=\frac{\xi^{-2}(t)}{\xi^{-2}[\bar{t}]},\quad w[\bar{t}]=\frac{\omega}{2\Gamma[\bar{t}]\xi^{-4}[\bar{t}]}.\quad (3.14)$$

Inserting into Eq. (3.3) finally we get

$$\mathcal{C}_s^2(t,\omega)=\left(\frac{\partial P}{\partial\rho}\right)_{\sigma\,[\bar{t}]}\times\frac{1+(\gamma_q^2[\bar{t}]/a_q)F_+^{(s)}(u[\bar{t}])}{1+(\gamma_q^2[\bar{t}]/a_q)F_+(v[t,\bar{t}],w[\bar{t}],\{\Xi[\bar{t}]\})}.\quad (3.15)$$

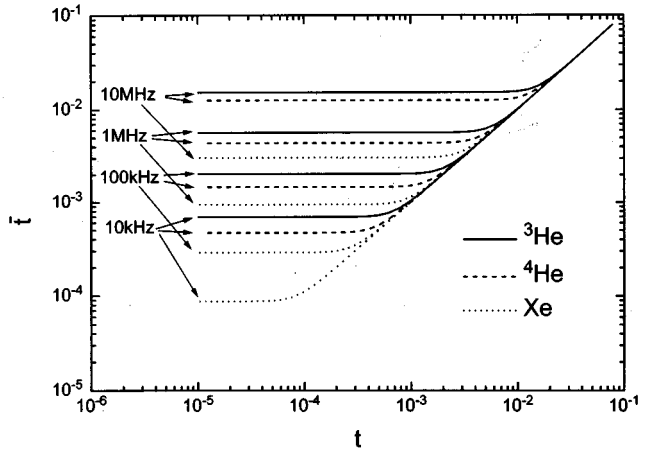

FIG. 1. The effective temperature distance $\overline{t}(t)$ [see Eq. (3.13)] as function of the temperature distance t at finite frequency for several fixed frequencies and liquids.

The explicit expression of the frequency-dependent amplitude function $F_+(v,w,\{\Xi\})$ is given in Eq. (3.4). The calculation of the static couplings $\gamma_q(\overline{t})$, $u(\overline{t})$ and the thermodynamic derivative $(\partial\rho/\partial P)_\sigma(\overline{t})$ at the zero frequency temperature scale from experimental quantities and the explicit expression of the static amplitude function $F_+^{(s)}(u)$ will be treated in the following section.

IV. DETERMINATION OF THE STATIC PARAMETERS

The flow parameter dependence and the temperature dependence respectively of the static couplings $u(t)$ and $\gamma_q(t)$ may in principle be calculated from the corresponding flow equations (I.4.8) and (I.4.9) together with the condition (I.4.15) fixing the connection between flow parameter and reduced temperature. However, in the region where the parameters adopt their background values, another procedure, that finds the static parameters directly from experiment, without using the flow equations is more appropriate. This method has been developed and successfully used at the λ transition in ^{4}He [14] and in ^{3}He-^{4}He mixtures [15]. It allows one to calculate the temperature-dependent model parameters from experimentally measured quantities by deriving relations between the ζ functions and thermodynamic functions. Equation (I.2.14) relates the adiabatic compressibility to the unrenormalized secondary density correlation function calculated within the model (I.2.10). To obtain a connection to renormalized parameters one has to search for expressions containing the correlation in which no explicit renormalization constants appear when the renormalized quantities are inserted. This requirement is fulfilled by the expressions

$$R_0(t)=\frac{(\partial\rho/\partial P)_\sigma^+}{(\partial\rho/\partial P)_\sigma^-},\quad \Delta_0^+(t)=-\frac{d\ln(\partial\rho/\partial P)_\sigma^+}{d\ln t}. \tag{4.1}$$

The superscript $+$ or $-$ indicates whether the quantity is taken above or below the critical temperature. The thermodynamic derivatives are related to the model correlation functions defined in (I.2.12). After a lengthy calculation given explicitly in [14] one ends up with the relations

$$\frac{R_0(t)-1}{\Delta_0^+(t)}=\frac{[2-\zeta_{\phi^2}(u)][F_-^{(s)}(u)-F_+^{(s)}(u)]}{B_{\phi^2}(u)-[2\zeta_{\phi^2}(u)-\epsilon]F_+^{(s)}(u)-\beta_u(u)dF_+^{(s)}/du} \tag{4.2}$$

$$\frac{\gamma_q^2(t)}{a_q}=\frac{[2-\zeta_{\phi^2}(u)]\Delta_0^+(t)}{B_{\phi^2}(u)-\{2\zeta_{\phi^2}(u)-\epsilon+[2-\zeta_{\phi^2}(u)]\Delta_0^+(t)\}F_+^{(s)}(u)-\beta_u(u)dF_+^{(s)}/du}, \tag{4.3}$$

where we have introduced

$$\zeta_{\phi^2}(u)=\zeta_r(u)-\zeta_\phi(u),$$

$$\beta_u(u)=u[-\epsilon-2\zeta_\phi(u)+\zeta_u(u)]. \tag{4.4}$$

The ζ functions have been defined in (I.4.6). $F_+^{(s)}$ and $F_-^{(s)}$ are the amplitude functions of the ϕ^2-ϕ^2 correlation function above and below T_c introduced in (I.4.19). The function B_{ϕ^2} follows from the additive renormalization of the ϕ^2-ϕ^2 correlation function [14] and $\epsilon=4-d$ is the standard dimensional parameter. Equation (4.2) allows the calculation of $u(t)$ from experimental quantities, because the right hand side of the equation only contains functions of u calculated within the ϕ^4 model (I.2.18), while the left hand side is related to thermodynamic derivatives. Solving the equation for u one gets the parameter expressed by thermodynamic functions. Inserting $u(t)$ in Eq. (4.3), one obtains $\gamma_q(t)$ with the same thermodynamic functions used before. In one loop order the ζ functions and amplitude functions for a one component order parameter read

$$\zeta_r=\frac{u}{2},\quad \zeta_u=\frac{3}{2}u, \tag{4.5}$$

$$\zeta_\phi=0,\quad B_{\phi^2}=\frac{1}{2}, \tag{4.6}$$

$$F_+^{(s)}=-\frac{1}{4},\quad F_-^{(s)}=\frac{3}{u}-1. \tag{4.7}$$

Inserting Eqs. (4.5)–(4.7) into the right hand side of Eqs. (4.2) and (4.3) one gets explicit expressions of u-dependent functions.

The adiabatic compressibility is not directly measurable in experiment; it is related to the experimental measurable quantities by

$$\left(\frac{\partial\rho}{\partial P}\right)_\sigma = \frac{C_V}{C_P}\left(\frac{\partial\rho}{\partial P}\right)_T, \tag{4.8}$$

with the isobaric specific heat

$$C_P = C_V + \frac{T}{\rho^2}\left(\frac{\partial P}{\partial T}\right)_\rho^2 \left(\frac{\partial\rho}{\partial P}\right)_T. \tag{4.9}$$

In contrast to the λ transition in ^{4}He [14] and ^{3}He-^{4}He mixtures [15] where only the knowledge of the temperature-dependent specific heat was necessary for the calculation of u and γ_q, now in the case of the gas-liquid transition we need the experimental information about the temperature behavior of three thermodynamic derivatives.

For an explicit calculation of C_P, $\gamma(t)$, and $u(t)$ Eqs. (4.9) and (4.8) offer two possible ways to proceed.

(i) Using experimental information about C_V, $(\partial\rho/\partial P)_T$, and $(\partial P/\partial T)_\rho$ one may immediately calculate C_P and $(\partial\rho/\partial P)_\sigma$ from Eqs. (4.9) and (4.8). From the latter quantity also γ_q^2/a_q can be calculated from Eq. (4.3) under the approximation $u(t)=u^\star$. This is justified since no explicit u contributions appear in the dynamic flow equations (2.11), (2.12) and the expressions for the transport coefficients (2.1), (2.3), and (3.15).

(ii) The thermodynamic derivative $(\partial\rho/\partial P)_\sigma$ may also be determined directly from sound velocity measurements at zero frequency by $(\partial\rho/\partial P)_\sigma = 1/c_s^2(\omega=0)$. In this case the static parameter γ_q^2/a_q is completely determined by the sound velocity at zero frequency. From Eq. (3.15) the sound attenuation and velocity at arbitrary finite frequency follow immediately. In order to obtain C_P, which is necessary for a calculation of the thermal conductivity, one needs additional experimental information about C_V and $(\partial\rho/\partial P)_T$ as can be seen from Eq. (4.8).

Thus for the calculation of the critical sound propagation we need either experiments on three temperature-dependent thermodynamic derivatives or measurements of the sound velocity at zero frequency in the critical region. For ^{3}He and ^{4}He the three thermodynamic derivatives C_V, $(\partial\rho/\partial P)_T$, and $(\partial P/\partial T)_\rho$ are available. In both liquids measurements of the zero frequency sound velocity also exist, which offers the possibility to compare the results of the two methods for a calculation of the critical sound velocity discussed above.

The isochoric specific heat in the critical region has been measured by Brown and Meyer [18] for ^{3}He and by Moldover [19] for ^{4}He. The data are shown in Fig. 2(a). In order to obtain a continuous representation of the experimental results we use the fit given in [18] for ^{3}He containing the correct asymptotic behavior

$$C_V = \frac{1+t}{T_c} t^{-\alpha}[A_1 + A_2 t^\Delta]. \tag{4.10}$$

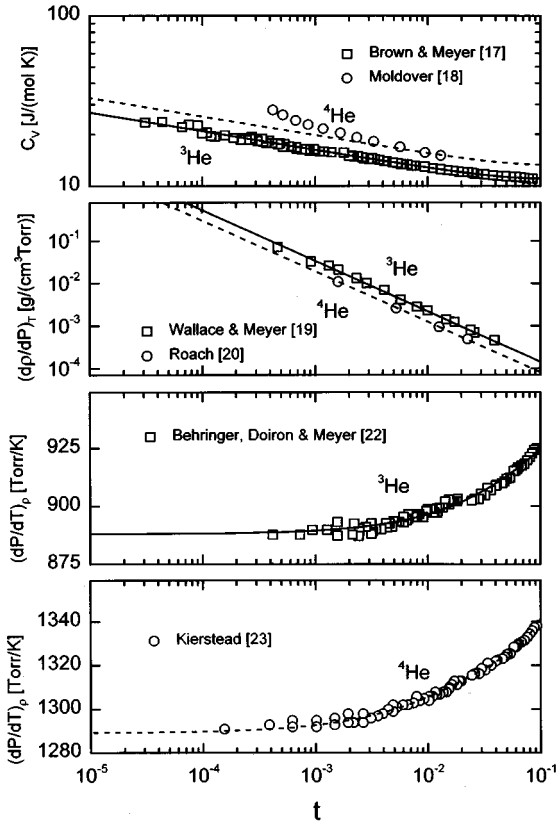

FIG. 2. Experimental thermodynamic derivatives in ^{3}He measured by [18,20,23] (squares) and ^{4}He measured by [19,21,24] (circels), which are used to determine the static coupling γ_q^2/a_q. The fits with expressions (4.10), (4.11), and (4.12) are drawn as full lines for ^{3}He and dashed lines for ^{4}He.

The critical exponents are fixed to $\alpha=0.11$ and $\Delta=0.54$, while the free parameters A_1 and A_2 are listed in Table II for both liquids. In ^{4}He the same expression (4.10) has been used with the parameter A_1 chosen to match the experimental data in the background and A_2 kept fixed at the ^{3}He value, because the increase in the region $t<10^{-2}$ seems to be too large compared with ^{3}He [see Fig. 2(a)]. Not all data of Ref. [19] have been shown since the data nearest to T_c are not consistent with a power law and an inclusion of the data below $t<10^{-2}$ shown here would lead to a value of $\alpha=0.15$.

The isothermal compressibility has been measured by Wallace and Meyer [20] for ^{3}He and by Roach [21] for ^{4}He. In both cases the data may be represented by a simple power law

$$\frac{1}{\rho_c}\left(\frac{\partial\rho}{\partial P}\right)_T = \Gamma_T t^{-\gamma}, \tag{4.11}$$

where the effective critical exponent is chosen to be $\gamma=1.19$ in the temperature region considered. This value is different from the expected asymptotic universal exponent 1.24 due to nonasymptotic effects. The amplitude Γ_T is determined by a fit, which is shown in Fig. 2(b) for both liquids. The parameters Γ_T obtained are listed in Table II [22]. Finally the thermodynamic derivative $(\partial P/\partial T)_\rho$ is found from measurements of the equation of state performed by Behringer *et al.*

TABLE II. Results for the fit parameters of Eqs. (4.10), (4.11), and (4.12) in ^{3}He and ^{4}He. The corresponding curves are shown in Fig. 3.

	A_1 (J/mol)	A_2 (J/mol)	Γ_T (1/Torr)	a_0 (Torr/K)	a_1 (Torr/K)	a_2 (Torr/K)	B (Torr/K)
^{3}He	25.11	2.6	2.23×10^{-4}	888.9	−1294.1	0.0	1289.0
^{4}He	48.0	2.6	7.53×10^{-5}	1289.2	−5190.5	4505.0	4085.7

[23] in ^{3}He and by Kierstead [24] in ^{4}He. The thermodynamic derivative is a smooth function of the temperature reaching a finite value at T_c. In order to get a continuous representation of the data in the considered temperature region we simply parametrize the thermodynamic derivative with

$$\left(\frac{\partial P}{\partial T}\right)_\rho = a_0 + a_1 t + a_2 t^2 + B t^{1-\alpha}. \tag{4.12}$$

The last term in Eq. (4.12) contains the correct asymptotic behavior of $(\partial P/\partial T)_\rho$ at the critical isochore [23]. The quantity itself is finite at the critical temperature but the temperature derivative diverges with the exponent of the specific heat α in the asymptotic limit. a_0 is determined by the value of $(\partial P/\partial T)_\rho$ at T_c [23]. The parameters a_1, a_2, and B are found by a fit shown in Figs. 2(c) and 2(d), and the parameters obtained are listed in Table II. The isobaric specific heat can now be calculated from the relation (4.9) by inserting the fits (4.10), (4.11), and (4.12) for ^{3}He and ^{4}He.

Inserting the three fits into Eqs. (4.8), (4.1), and (4.3) we obtain the static coupling γ_q^2/a_q shown in Fig. 3 as dashed lines for ^{3}He and ^{4}He. On the other hand from sound velocity measurements in ^{3}He [12] and in ^{4}He [25] we may directly calculate $(\partial\rho/\partial P)_\sigma$ from the experimental values shown in Fig. 4. The experimental data may be represented by a fit, shown as full lines in the same figure, with the asymptotic power law including first order corrections in the nonasymptotic region, which reads

$$\left(\frac{\partial \rho}{\partial P}\right)_\sigma = t^{-\alpha}(g_1 + g_2 t^\Delta). \tag{4.13}$$

The parameters g_1 and g_2 obtained by a fit in the region $10^{-5} \leqslant t \leqslant 10^{-1}$ for ^{3}He and $10^{-4} \leqslant t \leqslant 10^{-1}$ for ^{4}He are listed in Table III.

There are also measurements of the zero frequency sound velocity in the critical region for Xe [26], CO_2 [27], and SF_6 [28]. The resulting experimental derivative $(\partial\rho/\partial P)_\sigma$ and a fit over all data with Eq. (4.13) are also shown in Fig. 4, the parameters obtained are given in Table III. Inserting $(\partial\rho/\partial P)_\sigma$ from the sound velocity into Eq. (4.3) we get the static couplings γ_q^2/a_q for the three liquids shown in Fig. 3 as full lines. In the limit $t\to 0$ all curves reach a fixed point value that is different from the value obtained in one loop theory although we have used the one loop expressions for ζ functions. The reason for this behavior is, that we have fitted the thermodynamic derivatives with exponents different from the one loop exponents, which represent the experimental data in the considered temperature region in a more adequate way. For α and ν and Δ we used the best values available obtained in an asymptotic theory by higher order calculations. In contrast the exponent γ describing the temperature behavior of the isothermal compressibility in the experimentally accessible temperature region has been replaced by an effective one. The asymptotic region of that quantity obviously lies in a temperature region so close to the critical point that it is not reached by experiments.

V. COMPARISON OF THE TRANSPORT COEFFICIENTS WITH EXPERIMENT

A. Background parameters and thermal mode

We now determine the initial values of the Onsager coefficient Γ_0 and the mode coupling f_0. It is suitable to fit for that purpose the experimental measured shear viscosity with Eq. (2.10). Together with the results from statics discussed in the previous section the remaining transport coefficients like thermodiffusion coefficient or thermal conductivity as well as the sound velocity and the sound attenuation are then determined without any adjustable parameter. The reason for choosing the shear viscosity as the quantity to be fitted is the absence of any temperature-dependent static function in Eq. (2.10), which assures that the dynamic coefficients Γ_0 and f_0 are calculated from a pure dynamic function avoiding any mixing with static effects apart from the correlation length ξ. However, the amplitude ξ_0 influences the fit parameters found. As already mentioned the crossover of ξ to its background value ξ_b would also be of relevance. For most of the liquids the shear viscosity in the critical region is available

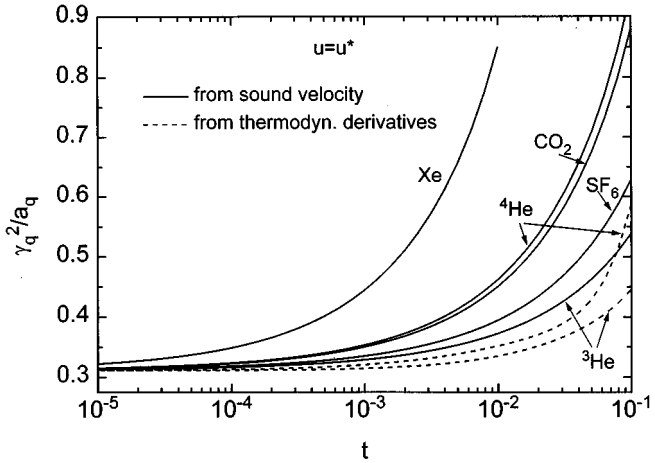

FIG. 3. A comparison of the static coupling γ_q^2/a_q calculated with Eq. (4.3) for several liquids. The two dashed lines are calculated with Eq. (4.8) inserting the thermodynamic derivatives (4.10), (4.11), and (4.12) for ^{3}He and ^{4}He. The full lines are determined from the adiabatic compressibility, which has been calculated from the zero frequency sound velocity in ^{3}He, ^{4}He, Xe, CO_2, and SF_6.

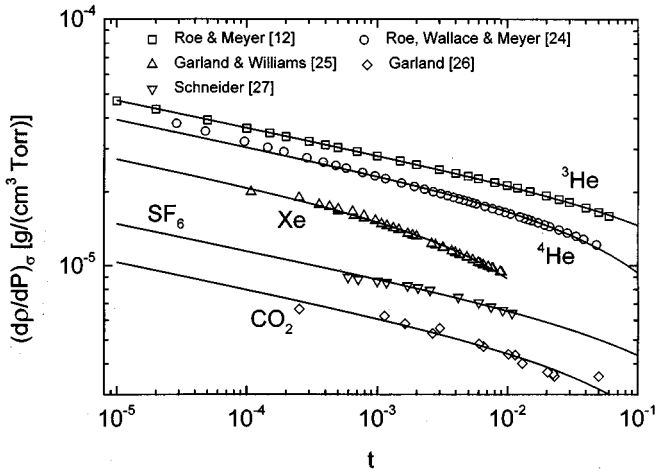

FIG. 4. The adiabatic compressibility determined from zero frequency experiments in ^{3}He [12] (squares), ^{4}He [25] (circles), Xe [26] (up triangles), CO_2 [27] (diamonds), and SF_6 [28] (down triangles). The corresponding fits with expression (4.13) are drawn as full lines.

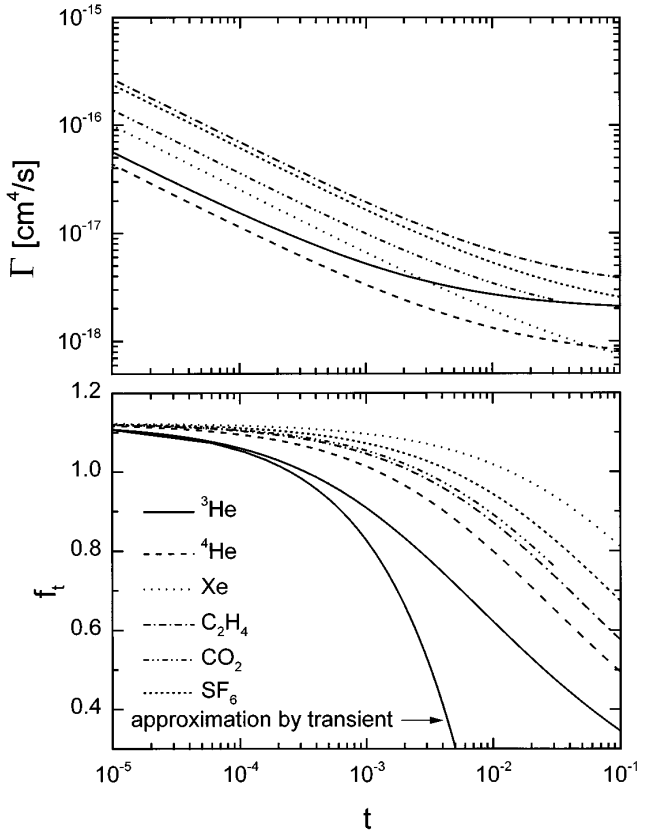

FIG. 5. Solutions of the flow equations (2.13) and (2.14) for several liquids where the initial values Γ_0 and f_0 have been found from fits of the shear viscosity (see Fig. 6 except for SF_6, where we fitted the thermal diffusion coefficient, see Fig. 7). The fit of the shear viscosity of C_2H_6 has already been shown in [31]. The corresponding initial values are listed in Table IV. For ^{3}He we also show the flow of f_t including only the first transient [according to Eq. (2.15)]. The restriction of this approximation to the near asymptotic region is clearly seen.

TABLE III. Results for the fit parameters of Eq. (4.13) for several liquids. The corresponding curves are shown in Fig. 5.

	$g_1\left[10^5 \frac{\text{g}}{\text{cm}^3\,\text{Torr}}\right]$	$g_2\left[10^5 \frac{\text{g}}{\text{cm}^3\,\text{Torr}}\right]$
^{3}He	1.331	−0.675
^{4}He	1.113	−1.344
Xe	0.773	−2.872
CO_2	0.292	−0.327
SF_6	0.418	−0.286

rather than the thermal diffusion coefficient or the thermal conductivity. The thermal diffusion coefficient is in most cases less suitable for the determination of the initial parameters because of the stronger temperature dependence masking the crossover behavior to the background.

In ethane (C_2H_6) both the shear viscosity [29] and the thermal diffusion coefficient [30] have been measured in sufficient accuracy for an analysis. The initial conditions obtained from the shear viscosity at the temperature distance t_0 are listed in Table IV although we do not present the fit of the shear viscosity and the prediction of the thermal diffusion coefficient. This has already been shown in [31] (see Fig. 2 there). For comparison with other liquids we show in Fig. 5 the corresponding flow of $\Gamma(t)$ and $f_t(t)$. Analogous to C_2H_6 we have fitted the experimental results of the shear viscosity in ^{3}He, ^{4}He [32], Xe [33], and CO_2 [34] in the temperature region indicated in Fig. 6 with Eq. (2.1). The resulting fits are shown in Fig. 6 as full lines and the initial values of Γ_0 and f_0 obtained are given in Table IV. The flows of the dynamic parameters $\Gamma(t)$ and $f(t)$ are compared in Fig. 5. Both the Onsager coefficient and the mode coupling are in the experimental region more or less different from their asymptotic behavior, most pronounced in ^{3}He and less pronounced in Xe.

No shear viscosity is available in SF_6 and therefore we use the data of the thermal diffusion coefficient [30]. The asymptotic temperature dependence of the thermal diffusion constant is given by a power law $D_T \sim t^{\gamma - x_\lambda \nu}$. The one loop value of the dynamical critical exponent $x_\lambda = \frac{18}{19} = 0.947$, which is somewhat larger than the two loop value $x_\lambda = 0.916$ [2]. This leads (i) to a flatter decrease in the thermal diffusion coefficient and (ii) a flatter increase in the shear viscosity in one loop order. However, since we only know the nonasymptotic amplitudes in one loop order we also keep the one loop order results for the flow equations and exponents. This deviation is seen in Fig. 7, where the fit region is again indicated by the bar. A similar deviation has been observed in the shear viscosity of CO_2 in the region $t < 10^{-5}$ not shown here. The asymptotic divergence of the shear viscosity $t^{-x_\eta \nu}$ is weaker because of $x_\eta = 0.053$ in one loop order and $x_\eta = 0.065$ in two loop order. In He this effect is masked by the gravitation. One might suggest to take in our analysis the two loop result for the flow equations. This, however, would lead, because of the change in the fixed point value of the mode coupling $f_t^\star$, to an inconsistent value of the Kawasaki amplitude R [7] known only in one loop order ($R^\star = 1.056$ [31]). Its nonasymptotic form enters the theory, when the shear viscosity is related to the thermal diffusion

TABLE IV. Initial values at t_0 of the dynamic model parameters Γ_0 and f_0 together with the asymptotic amplitude Γ_{as} of $\Gamma(t)$ according to Eq. (2.17) and the crossover temperature t_c at $\omega=1$ MHz.

Liquid	t_0	$\Gamma_0\left[10^{18}\frac{\text{cm}^4}{\text{s}}\right]$	f_0	$\Gamma_{as}\left[10^{18}\frac{\text{cm}^4}{\text{s}}\right]$	$10^{-3}\,t_c(1\text{ MHz})$
C_2H_6	0.1	3.87	0.576	0.276	0.87
^{3}He	0.1	2.11	0.345	0.057	4.3
^{4}He	0.1	0.83	0.495	0.044	2.7
Xe	0.1	0.75	0.811	0.1	1.6
CO_2	0.03	2.41	0.763	0.143	0.95
SF_6	0.1	2.56	0.674	0.246	1.1

$\overline{\eta}(t)=k_BTR(t)/[D_T(t)\xi(t)]$ according to Eqs. (2.5) and (2.10). Our asymptotic one loop value is also consistent with the optimal value adopted in mode coupling theory [13].

Now all dynamic parameters are determined and we are able to predict other transport coefficients. For C_2H_6 we have compared with the thermal diffusion coefficient (see Fig. 2 in [31]) and good agreement has been found. In ^{3}He and ^{4}He the thermal conductivity has been measured in the critical temperature region by Pittman *et al.* [35] (^{3}He) and by Acton and Kellner [36] (^{4}He). The experimental results are shown in Fig. 8. With the initial values given in Table IV we predict the thermal conductivity with Eqs. (2.2) and (2.3) for both liquids (full and dashed lines in Fig. 8). The isobaric specific heat has been calculated from Eq. (4.9) using method (i) explained in the preceding section. The slight minimum in the prediction for ^{3}He is an artifact resulting from the overcompensation of the decrease of $\Gamma(t)$ and $C_P(t)$ [see the expressions (2.5) and (2.2)] due to the increase of $\xi^{-2}(t)$ used in its asymptotic form in the region near the background, which is too strong. One should also note that a further extrapolation into the asymptotic region is not possible because here we used for C_P an effective exponent of $\gamma=1.19$ but $\nu=0.63$. It would be worthwhile to have more accurate static data for the isothermal compressibility. For CO_2, SF_6, and Xe we have no complete set of data available. Although in CO_2 the thermal conductivity has been measured one needs the static thermodynamic functions for a calculation of $C_P(t)$. No measurements of the thermal conductivity or thermal diffusion in SF_6 and Xe are known to us.

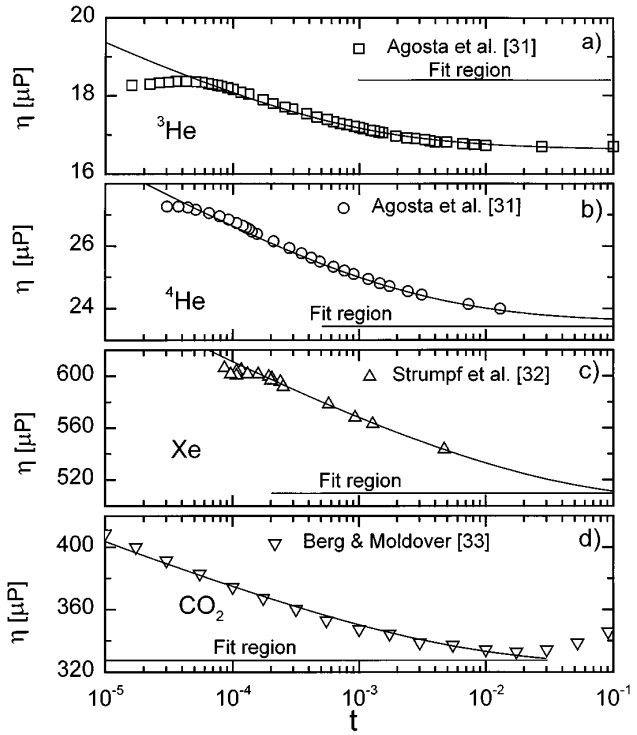

FIG. 6. Fits of the shear viscosity data of ^{3}He, ^{4}He [32], Xe [33], and CO_2 [34] with Eq. (2.4). The temperature intervals in which the fits have been performed are marked by a horizontal bar. The deviation of the fit in ^{3}He and ^{4}He below $t<10^{-4}$ indicates the onset of the influence of gravitation on the measurements not taken into account in this analysis. For Xe and CO_2 this influence is less pronounced.

As discussed in Sec. III the flow of all model parameters at finite frequency is calculable from the corresponding flow at zero frequency. Using Eq. (3.13) together with the flow of the Onsager coefficient $\Gamma(t)$ just determined we calculated at each temperature distance t for finite frequency the effective temperature distance $\overline{t}(t)$ via the matching condition (3.13). Since the dynamic nonasymptotic Onsager coefficient $\Gamma(\overline{t})$ enters the result of $\overline{t}$ is different from what one would get from the matching condition in its asymptotic form. The difference between the asymptotic matching condition and the nonasymptotic one has been discussed in [37]. For that pur-

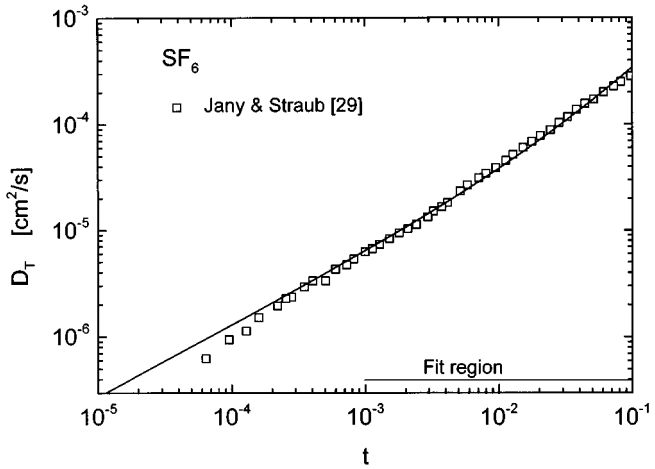

FIG. 7. Fit of the thermal diffusion coefficient data of SF_6 [30] with Eq. (2.5).

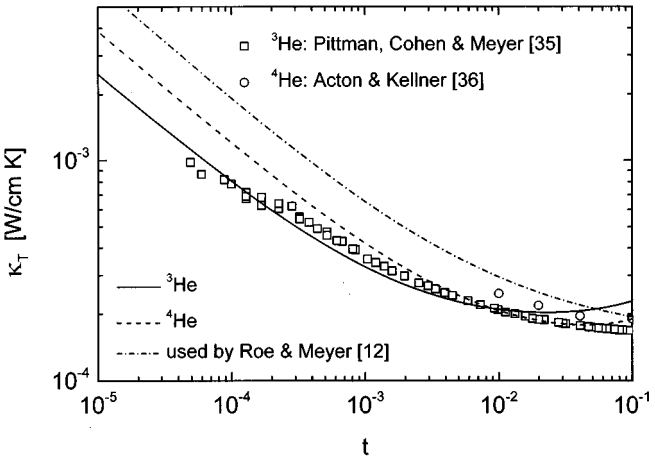

FIG. 8. A comparison of the experimental thermal conductivity in ^{3}He [35] (squares) and in ^{4}He [36] (circles) and predictions of the theory; the full line for ^{3}He and dashed line for ^{4}He are calculated from Eqs. (2.2) and (2.5) without any free parameter. The dashed-dotted line is the representation of the thermal conductivity for ^{3}He (at that time not measured) used in [12] [see Eq. (20) there] for the calculation of the scaled frequency $\tilde{y}$ appearing in the nonasymptotic scaling function for the reduced sound attenuation and sound dispersion.

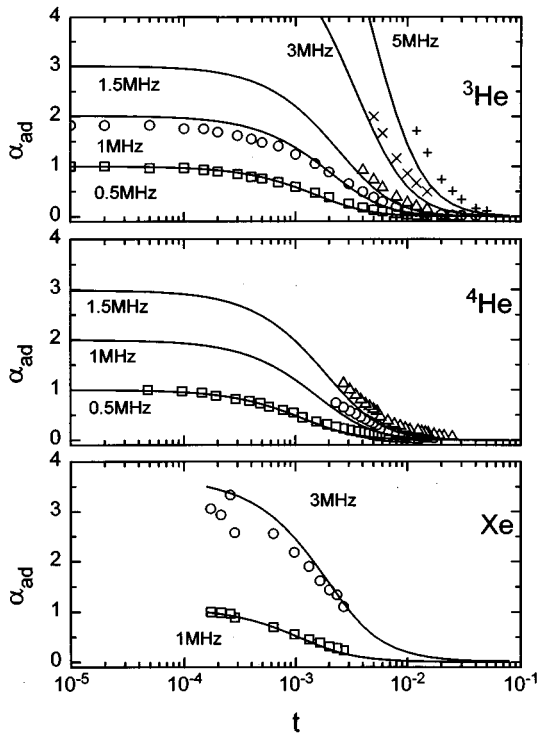

FIG. 9. Adjusted sound attenuation $\alpha_{ad}(t,\omega) = \alpha(t,\omega)/\alpha(t_n,\omega_n/2\pi)$ calculated from Eqs. (3.1), (3.2), and (3.15) without any adjustable parameter in ^{3}He, ^{4}He, and Xe (full lines). t_n is the temperature distance of the data point nearest to T_c at $\omega_n = 0.5$ MHz for He and $\omega_n = 1$ MHz for Xe. The experimental data are from [12] (^{3}He), [25] (^{4}He), and [39] (Xe).

pose one may replace $\Gamma(l)$ at a fixed distance from the critical point (measured in values of l) by its asymptotic power law behavior. The difference between the matching conditions (3.11) increases for an increasing distance from the critical point as can be seen in Fig. 6 of [37].

B. Sound mode

For a second test of the dynamic renormalization theory we turn to the prediction of the critical temperature dependence of the sound mode at finite frequencies. The question arises as to which extent the nonasymptotic flow, found in the comparison with the shear viscosity and the thermal mode, influences the sound mode. One has to note the following items: (i) the mode, coupling $f_t(l)$ does not appear in the expressions for the sound velocity and sound attenuation in one loop order according to Eq. (3.3); (ii) the order parameter Onsager coefficient $\Gamma(l)$ enters only via the matching condition Eq. (3.11) and the definition of $w(l)$ Eq. (3.6), (iii) the static coupling $\gamma_q(l)$ between the order parameter and the mass density enters at nonzero frequency. From this we expect that the main nonasymptotic effects found in the dynamic parameters can be taken into account by using a nonasymptotic scaled frequency (see Sec.VI below), whereas refined details depend on the nonuniversal behavior of the static coupling γ_q.

From Eqs. (3.1), (3.2), (3.14), and (3.15) we may now calculate the sound attenuation. The experimental sound attenuation is determined in terms of a signal ratio per length, which is given in Neper or dB. The absolute scale of our one loop theory can be judged by the value of the attenuation in one wavelength at T_c in the zero frequency limit, which is $0.2+O(f_t^2)$ according to (6.4) below and (I.7.7). The universal value without expandsion in f_t will be $\pi^2\alpha/2\nu z = 0.27$ [10]. In order to be independent of this value we normalize the attenuation at some frequency (we take the lowest available frequency) at some temperature value (we take the temperature value nearest to T_c). Dividing the sound attenuation by the value at its normalization point we get what we call adjusted attenuation α_{ad}. The same procedure is then done for our theoretical prediction. Thus apart from this normalization the adjusted attenuation at other frequencies and temperatures is then predicted. In Fig. 9 the comparison with the data is shown for ^{3}He [38], ^{4}He, and Xe [39]. For SF_6 a measurement only at one frequency is available but the predicted temperature dependence agrees quite satisfactorily with the data (see Fig. 10).

The crucial relation in the calculation of the theoretical adjusted sound attenuation is the matching condition (3.13), which determines at which temperature distance the effective temperature distance crosses over to a constant value (see Fig. 1). Within this crossover region the sound attenuation stops growing and bends over to its finite value at T_c. The location of this bendover is sensitive to the Onsager coefficient $\Gamma(\bar{t})$ found from the fit. A rough estimate of the crossover temperature can be found by comparing the two limiting matching conditions. At $t=0$ we have $2\omega/\Gamma(l) = (\xi_0^{-1}l)^4$ and at $\omega = 0$ we have $t^\nu = l$. Eliminating l leads to the estimate of the crossover temperature, $t_c \sim \sqrt{2\omega/\Gamma_{as}\xi_0^{-4}}$, where we have used the asymptotic Onsager coefficient and the approximations $z=3$ and $\nu = \frac{2}{3}$. For the frequencies considered in Fig. 9 the same quality of our prediction is reached whether the static coupling γ_q^2/a_q has been determined from the thermodynamic derivatives or from the zero frequency sound velocity as discussed in the

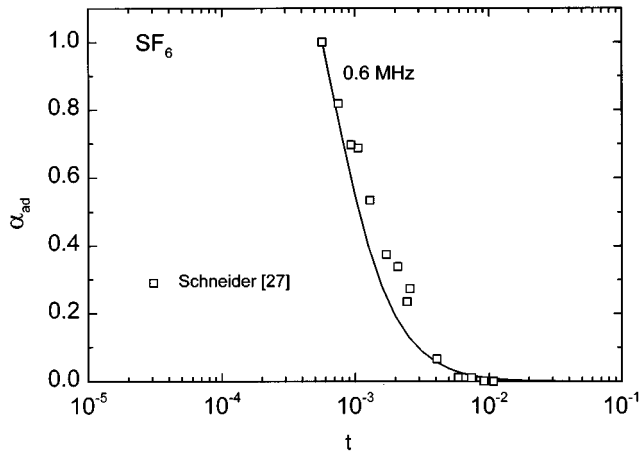

FIG. 10. Adjusted sound attenuation (same as in Fig. 9) calculated from Eqs. (3.1), (3.2), and (3.15) without any adjustable parameter in SF_6 (full line, $\omega_n = 0.6$ MHz). The experimental data are from [28].

previous section (see Fig. 3). The reason for this is the normalization of the sound attenuation data. Even at low frequencies the effective temperature distance reached lies in the nonasymptotic regime where γ_q^2/a_q is different from its universal asymptotic value [see the remark in paper I after (I.4.10)]. Thus the strong dependence of the attenuation on this static coupling, to which it is proportional, is weakened and most pronounced at large frequencies for ^{4}He (but smaller than 10%), because according to Fig. 3 there the difference due to the differences in the static measurements is largest.

From Eqs. (3.2), (3.14), and (3.15) the sound velocity at several frequencies has to be calculated. In contrast to the sound attenuation now the results may be influenced by the method of determining the static derivative $(\partial P/\partial\rho)_\sigma$. This is shown in Figs. 11 and 12. In Fig. 11 for ^{3}He and ^{4}He the lines are calculated using C_V, $(\partial\rho/\partial P)_T$, and $(\partial P/\partial T)_\rho$, while in Fig. 12 for ^{3}He, ^{4}He, Xe, and SF_6 the static derivative is determined from the experimental zero frequency sound velocity. One should note that the deviation in Fig. 11(a) of the theoretical sound velocity in ^{3}He calculated from static thermodynamic derivatives is of the order of 2% only. This can be considered as a proof of the internal consistency of the static experimental data [18,20,23]. In ^{4}He the deviation of the theoretical results is larger than in ^{3}He [see Fig. 11(b)]. One reason may be that the static thermodynamic derivatives, which are necessary to determine the model parameters, and the sound velocity itself are measured by different experimental groups [19,21,24,25] while in contrast in ^{3}He all data come from the same experimental group [18,20,23,32,12]. In Fig. 13 we present the prediction of the sound velocity of CO_2 calculated from the zero frequency sound velocity [27].

In the theory described above we have used the standard procedure in the calculation of the model functions. This means that the flow equations are taken in their full nonlinear form, and the amplitude functions of the transport coefficients have been calculated in an ϵ expansion [1]. Using the method mentioned in [40] one may avoid the ϵ expansion in the amplitude functions by calculating them directly at dimension $d=3$. This leads to somewhat different results for

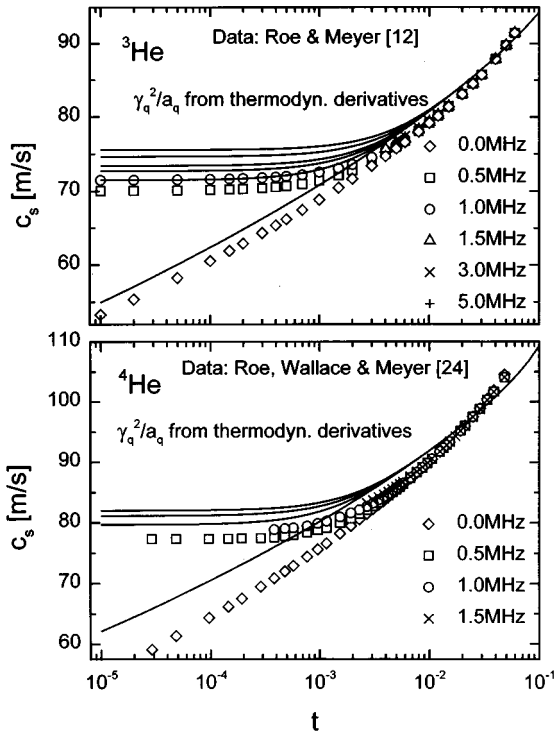

FIG. 11. Sound velocity in ^{3}He (data from [12]) and ^{4}He (data from [25]) at several frequencies without any free parameter. The curves are calculated from Eqs. (3.2) and (3.15) with the static coupling γ_q^2/a_q and the adiabatic compressibility extracted from the thermodynamic derivatives in Fig. 2.

the amplitude functions of the thermal diffusivity and the shear viscosity at zero frequency [compare Eq. (I.6.7)]

$$G(\{\Xi\}) = -\frac{f_t^2}{12}, \quad E_t(\{\Xi\}) = -\frac{f_t^2}{72}. \tag{5.1}$$

The frequency-dependent amplitude function F_+ of the $d=3$ calculation reads

$$F_+(v(l),w(l),\{\Xi(l)\}) = \frac{1}{2}\left\{\frac{v^{3/2}}{v_+v_-} + \frac{1}{v_+ - v_-} \times \left[\frac{v_-^{3/2}}{v_+} - \frac{v_+^{3/2}}{v_-}\right] - 1\right\}. \tag{5.2}$$

Performing a fit of the shear viscosity using the amplitude function E_t from Eq. (5.1) instead of the ϵ-expanded one, the sound attenuation and the sound velocity may be calculated with the $d=3$ amplitude function (5.2). The differences are a good estimate of the theoretical uncertainties at one loop level. To give an example we compare the results of the two calculations for the frequencies 0.5 and 1 MHz in ^{3}He in Fig. 14. Whereas the experimental data of the sound velocity lie within the two theoretical results, this is not the case for the sound attenuation, where the ϵ expansion seems to be more favorable. However, the differences are less than 10%.

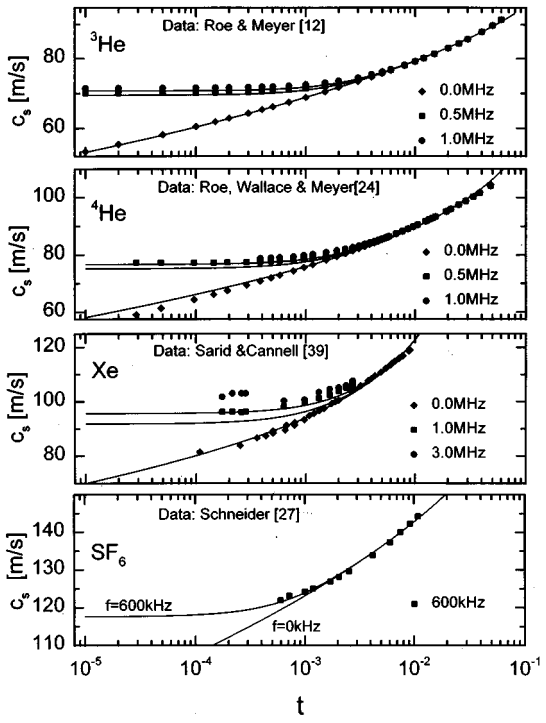

FIG. 12. Sound velocity in ^{3}He and ^{4}He (same data as in Fig. 11), Xe (data [39]), and SF_6 (data [28]). The curves are calculated from Eqs. (3.2) and (3.15) without any free parameter. The static coupling γ_q^2/a_q and the adiabatic compressibility been been extracted from the zero frequency sound velocity.

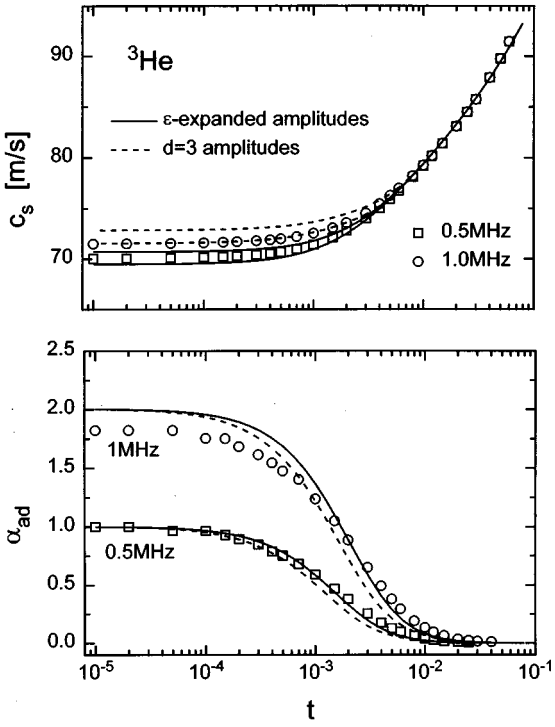

FIG. 14. Comparison of the sound attenuation and velocity calculated with the ϵ-expanded amplitude functions (3.4) (full lines) and the $d=3$ amplitude functions (5.2) (dashed lines) at 1 MHz in ^{3}He. The data (circles) are from [12].

VI. SCALING FUNCTIONS

A. Asymptotic scaling

We first consider the asymptotic limit of Eqs. (3.2) and (3.1). In this limit the order parameter Onsager coefficient follows a power law, $\Gamma(l)=\Gamma_{as} l^{z-4}$, with Γ_{as} from Eq. (2.17) and one introduces a scaled frequency y:

$$y=\frac{\omega}{2\Gamma_{as}\xi_0^{-4}t^{z\nu}}. \tag{6.1}$$

The matching condition Eq. (3.11) leads to the solution

$$l=t^{\nu}S(y) \tag{6.2}$$

with the limiting behavior $S(0)=1$ and $S(y)=(4y)^{1/z}$ close to T_c. An analytic solution of the matching condition (3.11) is possible if one takes the approximation $z=3$ for the dynamical critical exponent. This solution has been used for the calculation of the asymptotic scaling functions. A comparison of the asymptotic matching lines $l(t,\omega)$, where one uses the asymptotic power law behavior of $\Gamma(t)$, with the matching lines using the nonasymptotic solution for $\Gamma(t)$ definitively shows that the experimental data lie within the nonasymptotic region in the ω-t plane (see Fig. 6 in [37]). Therefore the application of these asymptotic results has to be taken with caution.

Inserting Eqs. (6.1) and (6.2) into the definition (3.6), the parameters v and w become functions of y:

$$v(l)=[S(y)]^{-2}, \quad w(l)=y[S(y)]^{-z}. \tag{6.3}$$

Then we obtain for the amplitude functions $F_+(y)$ and $\mathcal{C}_s(y)$ complex functions of y, from which the asymptotic crossover functions for the sound velocity $Y_c(y)$ [see (I.7.27)] and attenuation $Y_\alpha(y)$ [see (I.7.29)] are calculated. The crossover function for the sound velocity and the attenuation in one wavelength

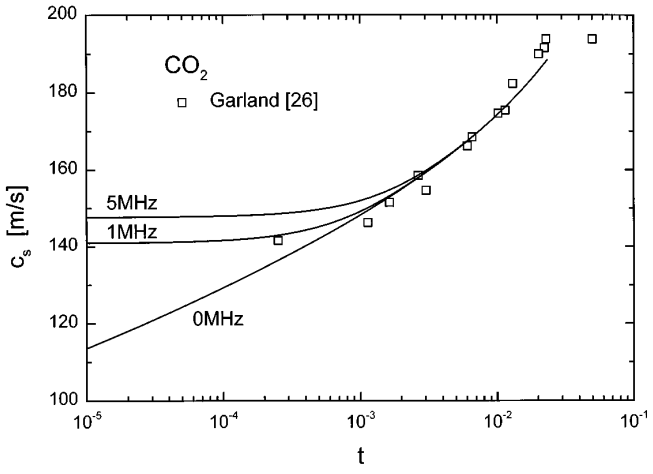

FIG. 13. Prediction of the sound velocity in CO_2 for different frequencies calculated as in Fig. 12. The zero frequency data are collected from [27].

$$\alpha\lambda = -\pi \frac{\mathrm{Im}[\mathcal{C}_s^2]}{\mathrm{Re}[\mathcal{C}_s^2]} \tag{6.4}$$

were shown in [37] (see Figs. 7 and 8 there). The last mentioned scaling function agrees quite well with the calculation of Ferrell and Bhattacharjee [10]. We note that because of the matching condition the whole range of values of the scaling variable $0 \leqslant y \leqslant \infty$ the scaling function is determined by values of the one loop integral contribution to $\mathcal{C}_s(v,w)$ and $F_+(v,w)$, with arguments within the region $0 \leqslant v(l) \leqslant 1$ and $0 \leqslant w(l) \leqslant \frac{1}{4}$.

B. Nonasymptotic scaling

Since it has been shown in our analysis of the experimental data that the behavior of the order parameter Onsager coefficient Γ and the mode coupling f_t is nonasymptotic, one may define, instead of the functions considered above, nonasymptotic scaling functions [12] by introducing the nonasymptotic scaled frequency

$$\tilde{y} = \frac{\omega}{2\Gamma(t)\xi^{-4}(t)}. \tag{6.5}$$

In the asymptotic limit $\tilde{y}$ turns into y. Plotting the suitable scaled attenuation in one wavelength and dispersion against the nonasymptotic scaled frequency the sound data fall almost on one curve [12]. A corresponding nonasymptotic scaling function can be found in our theoretical approach by solving the matching condition approximately. The approximation consists of replacing the l dependence in $\Gamma(l)$ by t^{ν} rather than $\overline{t^{\nu}}$ and keeping the nonasymptotic dependence of Γ on t. For the static coupling γ_q^2/a_q its fixed point value is taken. If ω is small compared to $\Gamma(l)\xi(t)^{-4}$ the solution of Eq. (3.11) may be written as

$$l = t^{\nu}\tilde{S}(\tilde{y}), \quad \tilde{S}(\tilde{y}) = (1+16\tilde{y}^2)^{1/8}. \tag{6.6}$$

Inserting l into the expressions for the complex coefficient $\mathcal{C}_s^2(t,\omega)$ we may plot the scaling functions for the reduced attenuation $I(\tilde{y})$ and reduced dispersion $J(\tilde{y})$ [see Eqs. (15) and (16) of [12] for the definition]

$$I(\tilde{y}) = -\pi \frac{\mathrm{Im}[\mathcal{C}_s^2(\tilde{y})]}{\tilde{S}^{\alpha/2\nu}(\tilde{y})\{\mathrm{Re}[\mathcal{C}_s^2(\tilde{y})]\}^2}$$

$$J(\tilde{y}) = 1 - \frac{\mathrm{Re}[\mathcal{C}_s^2(0)]}{\tilde{S}^{\alpha/\nu}(\tilde{y})\mathrm{Re}[\mathcal{C}_s^2(\tilde{y})]}, \tag{6.7}$$

with

$$v(l) = \frac{1}{\tilde{S}^2(\tilde{y})}, \quad w(l) = \frac{\tilde{y}}{\tilde{S}^4(\tilde{y})}. \tag{6.8}$$

The denominator in $w(l)$ is essential for the comparison with the data since it restricts the $w(l)$ values used in the expression for F_+ to the same finite interval $0 \leqslant w(l) \leqslant \frac{1}{4}$ as the asymptotic scaling function. The lowest order approximation $w(l) = \tilde{y}$ would introduce into $I(\tilde{y})$ and $J(\tilde{y})$ the behavior of F_+ for large values of the argument w and would lead to a decrease to zero for both nonasymptotic scaling functions. The correct solution of the matching condition prohibits this decrease and the reduced attenuation reaches a constant value (the same as the asymptotic scaling function) for large values of $\tilde{y}$ and y, respectively. As a consequence of the noniterative solution of the matching condition this approximation does not lead to the correct frequency behavior in the limit $t \to 0$ since $l = \omega^{1/4} t^{\nu x_\lambda/4}$ in the limit $\tilde{y} \to \infty$. Thus the temperature dependence of the sound attenuation and sound velocity does not drop out in this limit and the frequency dependence is the same as in the Van Hove theory ($z=4$). Nevertheless one may represent the data over a certain range of $\tilde{y}$ by such an approximative scaling function. In fact it turns out that the differences in the scaling functions plotted in the experimental range are small.

In order to compare now the scaling functions with the data of ^{3}He [12] we have to fix the scale of the frequency axis and of the ordinate. The relation of our nonasymptotic scaled frequency to the scaled frequency used in [12] is given by the choice of $\omega^{\star}$ of that paper, which is according to Eq. (2.5),

$$\omega^{\star} = \frac{\omega}{2D_T(t)\xi^{-2}(t)} = \frac{\tilde{y}}{1 - f_t^2(t)/16}. \tag{6.9}$$

One may replace f_t by its fixed point value leading to a denominator of 0.93. However, the thermal conductivity used to fix the scale in [12] does not represent the data measured later [35] (see dot-dashed curve in Fig. 8). Therefore we shifted the reduced attenuation along the $\tilde{y}$ axis to get agreement with our frequency scale [41]. A check of consistency is the plot of the reduced dispersion for which the same $\tilde{y}$ scale has been used. An additional shift along the ordinate has been performed in the reduced dispersion in order to normalize to our function. Excellent agreement is reached where expected (see Fig. 15). We also plot the corresponding asymptotic scaling functions. The differences show the uncertainty within the theory. The nonasymptotic scaling plot of the data has recently compared with an asymptotic calculation to $O(\varepsilon^2)$ [11] and qualitative similar results have been obtained.

The same remarks apply to the ^{4}He [25] (reanalyzed in [12]) and included in Fig. 15. The conclusion is that nonasymptotic effects are less pronounced seen in this double logarithmic scaling plots but our detailed analysis of Sec. V shows that consistency of the description for *all* hydrodynamic transport coefficients is possible within a nonasymptotic renormalization group theory only.

The nonasymptotic scaling function takes into account only nonasymptotic effects in the frequency scale; it neglects similar effects in the coupling γ_q^2/a_q by using the fixed point value for this coupling. These effects in the coupling are seen most directly at T_c, where the attenuation in one wavelength Eq. (6.4) reaches a finite universal value for small frequencies. At finite frequencies a nonuniversal value is observed and this value was related to the non-asymptotic behavior of the specific heat $C_V(t)$ by Bhattacharjee and Ferrell [10]. In our theory this effect is of the same physical origin and re-

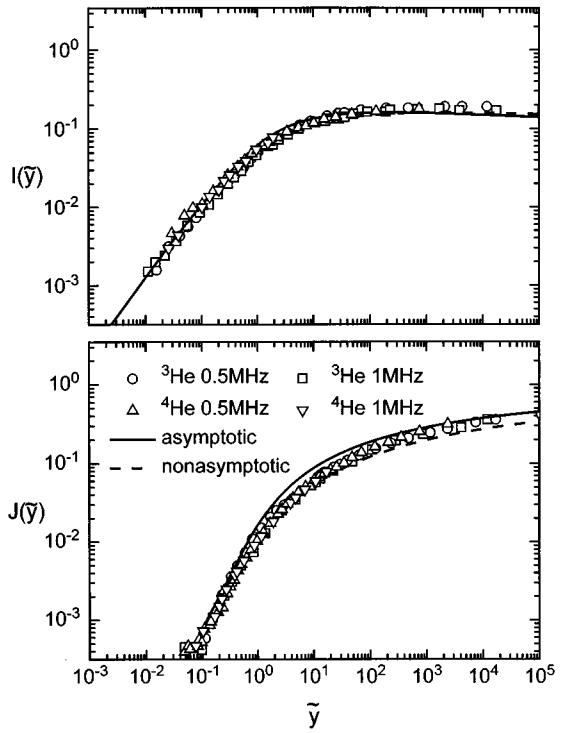

FIG. 15. Reduced sound attenuation $I(\tilde{y})$ and reduced dispersion $J(\tilde{y})$ as function of the nonasymptotic scaled frequency $\tilde{y}$. The asymptotic scaling function (full line) uses the solution (6.2) in (6.3) and the nonasymptotic scaling function (dashed line) the approximation (6.6) in (6.8).

lated to the deviation of the static coupling γ_q^2/a_q, shown in Fig. 3, from its fixed point value $\gamma_q^{\star 2}/a_q$. From Eq. (3.15) we calculate the ratio of the attenuation in one wavelength at finite frequency to the value at zero frequency at T_c:

$$\frac{\alpha\lambda}{(\alpha\lambda)_c}=\frac{\gamma_q^2(x)}{\gamma_q^{\star 2}}\,\frac{1+(\gamma_q^{\star 2}/4a_q)\ln 2}{1+[\gamma_q^2(x)/4a_q]\ln 2}, \tag{6.10}$$

where x is the effective temperature distance corresponding to the finite limiting value of the flow parameter l_c given in (I.71) and where we have used (I.7.7). We take for $\gamma_q^{\star 2}/a_q$ the experimental value 0.311 from Fig. 3. Figure 16 shows our result in comparison to the experimental values given in [10]. The nonasymptotics of the specific heat in [10] was characterized by the background noncritical contribution B; in our theory the whole experimental temperature dependence enters directly leading to a characteristic curve for each liquid. The steeper the decrease of the specific heat (or compressibility) the stronger the increase of the curve. However, we expect a saturation or bending over of the curves for larger values of x when the specific heat crosses over to its background value. Thus an improvement in agreement at least from this side is to expected, e.g., for Xe by more accurate measurements of the specific heat or zero frequency sound velocity.

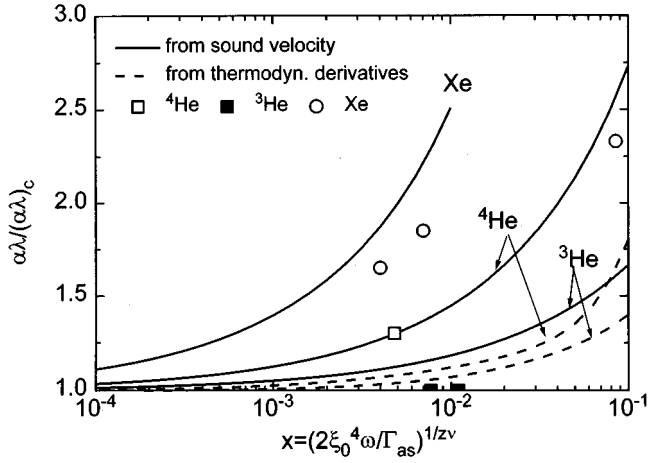

FIG. 16. The enhancement of the nonasymptotic high frequency attenuation in one wavelength at T_c for several fluids and different static input as function of scaled frequency. The data are taken from Ref. [10].

VII. CONCLUSION

We have performed a detailed analysis of the critical behavior of the hydrodynamic transport coefficients in a pure liquid. The nonuniversal nonasymptotic temperature dependence of the shear viscosity and/or thermal conductivity has been fully taken into account in the prediction of the temperature and frequency dependence of the sound velocity and sound attenuation. Refinements of the analysis are worthwhile and possible. (i) One needs more detailed information on the experimental side (i) on the correlation length (especially the crossover to a constant background value would be of interest), (ii) more accurate information on the static thermodynamic derivatives, and (iii) more complete sets of transport coefficients. The theory can be improved by a two loop calculation of the amplitude functions (however, not all integrals seem to be calculable analytically; see, e.g., [11]) and extended to the ordered phase (this would, e.g., make possible the prediction of the sound attenuation in the liquid and/or vapor phase).

A similar analysis is possible and in preparation in mixtures. However, it includes an additional dynamic parameter (a certain ratio of Onsager coefficients) because of the additional equation for the concentration fluctuation. This new dynamic parameter governs the critical enhancement of the thermal conductivity at zero mass current and is of importance in the nonasymptotic region [31,42]. It also enters the frequency scale of the sound mode.

Note added in proof. The asymptotic theory has been considered recently by A. Onuki [Phys. Rev. E **55**, 403 (1997)]. A comparison of our and Onuki's theory with sound data in ^{3}He and ^{4}He will be published by A. Kogan and H. Meyer in J. Low Temp. Phys. We thank the authors for sending us a preprint.

ACKNOWLEDGMENT

We thank H. Meyer for helpful discussions and for sending us his experimental data.

[1] R. Folk and G. Moser, preceding paper, Phys. Rev. E **57**, 683 (1997).
[2] E.D. Siggia, B.I. Halperin, and P.C. Hohenberg, Phys. Rev. B **13**, 2110 (1976).
[3] R. Dengler and F. Schwabl, Europhys. Lett. **4**, 1233 (1987).
[4] R. Folk and G. Moser, J. Low Temp. Phys. **99**, 11 (1995).
[5] V. Dohm, J. Low Temp. Phys. **69**, 51 (1987).
[6] J. Pankert and V. Dohm, Phys. Rev. B **40**, 10 842 (1989); **40**, 10 856 (1989).
[7] K. Kawasaki, Ann. Phys. (N.Y.) **61**, 1 (1970).
[8] D.M. Kroll and J.M. Ruhland, Phys. Lett. **80A**, 45 (1980).
[9] R.A. Ferrell and J.K. Bhattacharjee, Phys. Lett. **86A**, 109 (1981).
[10] J.K. Bhattacharjee and R.A. Ferrell, Phys. Lett. **88A**, 77 (1982).
[11] L.Ts. Adzhemyan, A.N. Vasiljev, and A.V. Serdukov, in Proceedings of the RG96-Conference, Dubna, August 1996 (World Scientific, Singapore, in press).
[12] D.B. Roe and H. Meyer, J. Low Temp. Phys. **30**, 91 (1978).
[13] J. Luettmer-Strathmann, J.V. Sengers, and G.A. Olchowy, J. Chem. Phys. **103**, 7482 (1995).
[14] V. Dohm, Z. Phys. B **60**, 61 (1985).
[15] G. Moser and R. Folk, J. Low Temp. Phys. **86**, 57 (1992); **86**, 99 (1992).
[16] J.V. Sengers and J.M.H. Levelt-Sengers, Annu. Rev. Phys. Chem. **37**, 189 (1986).
[17] If in the background the correlation length reaches its constant value ξ_b the matching condition leads to a flow parameter depending only on frequency. A simple approximation for not too large frequencies would be $l=\xi_0\{\xi_b^{-8}+[2\omega/\Gamma(\xi_0/\xi_b)]^2\}^{1/8}$.
[18] G.R. Brown and H. Meyer, Phys. Rev. A **6**, 364 (1972).
[19] M.R. Moldover, Phys. Rev. **182**, 342 (1969).
[20] B. Wallace, Jr. and H. Meyer, Phys. Rev. A **2**, 1563 (1970); C. Pittman, T. Dorion, and H. Meyer, Phys. Rev. B **20**, 3678 (1979). In the second reference a fit with $\gamma=1.24$ and correction terms is performed.
[21] P.R. Roach, Phys. Rev. **170**, 213 (1968).
[22] Note that we use the effective exponent $\gamma=1.19$ instead of $\gamma=1.16$ as in [20], which leads to a different value of Γ_T.
[23] R.P. Behringer, T. Doiron, and H. Meyer, J. Low Temp. Phys. **24**, 315 (1976).
[24] H.A. Kierstead, Phys. Rev. A **7**, 242 (1973).
[25] D.B. Roe, B.A. Wallace, and H. Meyer, J. Low Temp. Phys. **16**, 51 (1974).
[26] C.W. Garland and R.D. Williams, Phys. Rev. A **10**, 1328 (1974).
[27] C.M. Herget, J. Chem. Phys. **8**, 537 (1940); H.D. Parbrook and E.G. Richardson, Proc. Phys. Soc. London, Sect. B **65**, 437 (1952); H. Tilsch and H. Tanneberger, Z. Phys. **137**, 256 (1954); H. Tanneberger, *ibid.* **153**, 445 (1959).
[28] W.G. Schneider, J. Chem. Phys. **18**, 1300 (1950); **20**, 759(E) (1952).
[29] H. Iwasaki and M. Takahashi, J. Chem. Phys. **74**, 1930 (1981).
[30] P. Jany and J. Straub, Int. J. Thermophys. **12**, 165 (1987).
[31] R. Folk and G. Moser, Phys. Rev. Lett. **75**, 2706 (1995).
[32] C.C. Agosta, S. Wang, L.H. Cohen, and H. Meyer, J. Low Temp. Phys. **67**, 237 (1987).
[33] H.J. Strumpf, A.F. Collings, and C.J. Pings, J. Chem. Phys. **60**, 3109 (1974).
[34] R.F. Berg and M.R. Moldover, Phys. Rev. A **42**, 7183 (1990).
[35] E. Pittman, L.H. Cohen, and H. Meyer, J. Low Temp. Phys. **46**, 115 (1982).
[36] A. Acton and K. Kellner, Physica B **90**, 192 (1977); H. Meyer (private communication). See also H. Meyer and L.H. Cohen, Phys. Rev. A **38**, 2081 (1988).
[37] R. Folk and G. Moser, in Proceedings of the RG96 Conference (Ref. [11]).
[38] In [31] [see Fig. 1(c) there] the attenuation has been normalized at each frequency separately. Therefore the agreement at higher frequencies in Fig. 9 is ''less perfect'' than in the earlier presentation.
[39] D. Sarid and D.S. Cannell, Phys. Rev. A **15**, 735 (1977).
[40] R. Schloms and V. Dohm, Nucl. Phys. B **328**, 639 (1989).
[41] In fact one should replot the sound data with the correct nonasymptotic frequency scale. We do not expect substantial changes compared with those presented in Fig. 15.
[42] R. Folk and G. Moser, Condensed Matter Physics (Ukraine) **7**, 27 (1996).